Journal of Materials Chemistry A

Accepted Manuscript

ROYAL SOCIETY OF CHEMISTRY

www.rsc.org/materialsA

Journal of Materials chemistry A

ARTICLE

Mesoporous Fe/N/C oxygen reduction catalyst through NaCl crystallites-confined pyrolysis of polyvinylpyrrolidone

Wang Wang,[a] Jin Luo,[a] Huiwen Chen,[a] Jun Li,[a] Wei Xing,[b] Shengli Chen,[a,*]

Received 00th January 20xx,
Accepted 00th January 20xx

DOI: 10.1039/x0xx00000x

www.rsc.org/

Ternary Fe/N/C catalysts are regarded as the most promising candidate of low-cost alternative to Pt for catalyzing the oxygen reduction reaction (ORR). High-temperature pyrolysis of N-containing carbon precursors in the presence of Fe salts has been a common and efficient route to prepare the Fe/N/C catalysts. However, simple pyrolysis usually leads to large weight loss of N-containing precursor, which not only increases the overall cost of the catalysts, but also results in catalysts having low density of active sites. We show herein that this problem can be effectively overcome by dispersing a highly hydrosoluble polymer precursor, namely, the polyvinylpyrrolidone (PVP), in the NaCl crystallites. The use of the hydrosoluble polymer precursor enables efficient dispersing and confining of precursor in NaCl crystallites in a simple solvent evaporation process. The subsequent pyrolysis process not only shows little weight loss, but produces a mesoporous Fe/N/C ORR catalyst with remarkably higher specific surface area (414.5 $m^2 g^{-1}$) and ORR activity (half-wave potentials, $E_{1/2}$=0.793 V and 0.878 V vs. RHE respectively in acidic and alkaline media) than the material prepared without using the NaCl confinement (72.9 $m^2 g^{-1}$, $E_{1/2}$=0. 634 V and 0.785 V respectively in acidic and alkaline media), as well as superior stability under the ORR condition.

Introduction

Proton exchange membrane fuel cells (PEMFCs) have been regarded as one of the most promising energy conversion technologies available today.[1-12] However, the sluggish kinetics of oxygen reduction reaction (ORR) at the cathode requires the expensive Pt catalysts, which hinders the widespread application of PEMFCs.[13-20] Therefore, great efforts have been devoted to search for earth-abundant materials to catalyze ORR to substitute Pt-based catalysts.[21-26] Ternary Fe/N/C catalysts have attracted great interests in recent years because of the comparably high activity and four-electron-transfer selectivity towards ORR.[27-31] The studies on Fe/N/C catalysts can be traced back to the discovery of ORR activity of cobalt phthalocyanine reported by Jasinski in 1964,[32] initiating the investigation of other analogous metal-nitrogen coordinating macrocycles to improve the ORR activities. In 1980s, Yeager and coworkers proposed that the pyrolysis of the mixture of nitrogen-containing precursors and iron salts could form Metal-N_x catalytic sites,[33, 34] which led to the booming of Fe/N/C catalyst through the pyrolysis of various iron salts and nitrogen-containing species. Despite the significant advancements achieved by the elaborate selection of nitrogen and carbon precursors with effective carbonization process,[35, 36] the ORR performance of Fe/N/C catalyst in acidic electrolyte compared to Pt-based catalysts still needs to be further improved because of the fewer active sites and poor mass transport in the catalyst layer.[13, 37]

An effective way to increase the number of active sites and enhance the mass transport is to increase the surface area of the Fe/N/C catalyst. A large surface area with porous structure can make the active sites fully exposed to the interface, where electrons, protons, oxygen and product water can pass in or out rapidly, leading to much improved ORR activity and mass-transport properties which are critical for the whole fuel cell performance.[38, 39] However, directly pyrolizing the mixture of iron salts and nitrogen-containing precursors usually fails in developing highly active Fe/N/C catalysts with good mass-transport properties due to the lack of necessary porous structure. What's more, a large weight loss and nitrogen evaporation were generally observed during the direct pyrolysis of the precursor, which not only increases the overall cost of the catalysts, but also makes the resulting catalysts have low density of active sites.

Recently, Wei et al.[40] introduced a novel salt recrystallization method to seal polyaniline (PANI) inside the NaCl crystal which functions as a closed nanoreactor. During the pyrolysis, this nanoreactor can not only make use of the released gas inside the nanoreactor to create a large amounts of pores, but also delay the decomposition of the precursor to enhance the N incorporation and graphitization. The as-obtained catalyst has exhibited excellent ORR catalytic performance with a surface area of 265.7 $m^2 g^{-1}$. It demonstrated to be an effective and efficient method to synthesize Fe/N/C catalyst with the assistance of inorganic salts, such as NaCl, $ZnCl_2$.[41] It can be inferred that the key point of this method is to

[a] Hubei Electrochemical Power Sources Key Laboratory, Department of Chemistry, Wuhan University, Wuhan 430072, China. Tel./Fax: (+86) 27 6875 4693; E-mail: slchen@whu.edu.cn.
[b] State Key Laboratory of Electroanalytical Chemistry, Changchun Institute of Applied Chemistry, Chinese Academy of Sciences, Changchun, Jilin, 130022, China.

Electronic Supplementary Information (ESI) available: [details of any supplementary information available should be included here]. See DOI: 10.1039/x0xx00000x

efficiently confine the precursors in the NaCl crystal. Although PANI have been proved to be a promising precursor for the synthesis of Fe/N/C,[42] it might not be the most appropriate precursor applied to this method. Because of the poor solubility in water, the PANI tends to precipitate in aqueous media during the water evaporation. This will cause the phase separation of PANI and NaCl, thus leading to inefficient confining of PANI by NaCl crystals. Therefore, repeated sealing processes had to be used.[36]

To mitigate the phase separation problem, a highly soluble nitrogen-containing precursor—Polyvinylpyrrolidone (PVP), a widely used green surfactant — was employed in this work. For the precursor is highly soluble (100 g in 100 ml water), it will disperse homogeneously in the supersaturated NaCl solution and avoid agglomeration as the water evaporates off rapidly. In result, a porous Fe/N/C ORR catalyst (denoted as PVP-NaCl-Fe/N/C) was obtained by pyrolyzing a mixture of a highly hydrosoluble Polyvinylpyrrolidone (PVP) and $FeCl_3$ with the assistance of NaCl, which had a large specific surface area of 414.5 $m^2\ g^{-1}$, and remarkable ORR activity both in acidic and alkaline media, with half-wave-potentials ($E_{1/2}$) of 0.793 V and 0.878 V (vs. RHE) respectively. The PEMFC single cell, assembled with the prepared catalyst as the cathode (loading: 2 mg cm^{-2}), achieved a peak power density of 202 mW cm^{-2}. These results demonstrate that the Polyvinylpyrrolidone-based Fe/N/C ORR catalyst synthesized with the assistance of NaCl might be viable for high-performance fuel cells.

Experimental section

Synthesis of PVP-NaCl-Fe/N/C and PVP-Fe/N/C: PVP-NaCl-Fe/N/C was prepared by dissolving 1 g Polyvinylpyrrolidone (MW=29000, Sinopharm Chemical Reagent Co., Ltd.) and 20 mg $FeCl_3{\cdot}6H_2O$ (Sinopharm Chemical Reagent Co., Ltd.) in 15 mL saturated NaCl (Sinopharm Chemical Reagent Co., Ltd.) solution with vigorous stirring under 80 ℃ for about 40 min. Then the light yellow sample was transferred to ceramic crucible, and heat-treated under argon atmosphere at 900 ℃. After cooling to room temperature, the sample was washed with 0.5 M H_2SO_4 (Sinopharm Chemical Reagent Co., Ltd.) for 6 h and annealed at 900 ℃ again. The wash with H_2SO_4 can remove the inactive inorganic salts, and the second anneal is used to remove the possible defects formed during H_2SO_4 leaching. For comparison, PVP-Fe/N/C was prepared under the same condition without the adding NaCl.

Structure and morphology characterization: The structure and morphology of the prepared materials were characterized by Transmission Electron Microscope (TEM, JEM-2100F), Raman spectroscopy (Renishaw inVia, Renishaw, 532 nm excitation wavelength), and X-ray photoelectron spectroscopy (Kratos Ltd. XSAM-800). The N_2 adsorption isotherms were investigated by an ASAP2020 Surface Area and Porosity Analyzer (Micromeritics, USA). Thermogravimetric analysis (TGA) was conducted by a TGA Q500 (TA instrument, USA).

Electrochemical measurements: All electrochemical measurements were performed using a CHI 400 electrochemical workstation in a standard three-electrode cell with a Pt plate as the counter electrode, saturated calomel electrode (SCE) as the reference electrode when the 0.1 M $HClO_4$ was used as the electrolyte, Hg/HgO electrode as the reference electrode for measurements in 0.1 M KOH, and a glassy carbon (GC) rotating-disk-electrode (RDE) electrode (5 mm in diameter) loaded with catalyst sample as the working electrode. To prepare the working electrode, 5 mg sample catalyst was dispersed in 1 mL Nafion/isopropyl alcohol solution (0.1%) to form the catalyst ink by sonicating for 30 min; 20 μL of the ink was then pipetted onto the GC electrode. In comparison, working electrode loaded with 20 wt% Pt/C catalyst was also made, with 6 μL of Pt/C catalyst ink being pipetted onto the GC electrode. The potentials were reported with respect to the reversible hydrogen electrode (RHE). To calibrate the equilibrium potential of the SCE (Hg/HgO) electrode to RHE scale, the steady-state polarization curves of the hydrogen electrode reactions on Pt/C-loaded GC electrode in 0.1 M $HClO_4$ (or 0.1 M KOH) saturated with H_2 was measured; the RHE zero potential was estimated with the potential at which the current crossed zero. The RDE measurements were performed at different rotating speeds from 400 to 1600 rpm at a scan rate of 5 mV s^{-1}. Koutecky-Levich plots were used to investigate the effective electron-transfer number and the mass-transport corrected current density for ORR at different potentials. According to the Koutecky-Levich equation:

$$J^{-1} = J_k^{-1} + J_L^{-1} = J_k^{-1} + \frac{1}{B\omega^{1/2}} \quad (1)$$

$$\mathrm{B} = 0.62\mathrm{nF}C_0(D_0)^{2/3}\nu^{-\frac{1}{6}} \quad (2)$$

where J, J_K, J_L are the measured current density, kinetic current density and diffusion-limiting current density, respectively; ω is the electrode rotating speed, B is a constant relating to the electron transfer number (n), Faraday constant (F, 96485 C mol^{-1}), the diffusion coefficient of O_2 (D_0, 1.93×10^{-5} $cm^2\ s^{-1}$ for 0.1 M $HClO_4$), the concentration of O_2 in the solution (C_0, 1.2×10^{-3} mol L^{-1} for 0.1 M $HClO_4$) and the kinetic viscosity of the electrolyte (v, 0.01 $cm^2\ s^{-1}$ for 0.1 M $HClO_4$) . The kinetic current density was obtained after mass-transport correction by:

$$J_K = J \times J_L / (J_L - J)^{-1} \quad (3)$$

The rotating ring-disk electrode was employed to detect the H_2O_2 yield, where the ring potential was set to 1.2 V (vs. RHE). The H_2O_2 yield was calculated through the following equation:

$$H_2O_2\,(\%) = 200 \times \frac{I_{ring}/N_0}{(I_{ring}/N_0) + I_{disk}} \quad (4)$$

Where, I_{ring} and I_{disk} are the ring and disk currents, respectively. N_0 is the ring collecting efficiency, which was calibrated using 10 mM $K_3[Fe(CN)_6]$ in 0.1 M KNO_3. The measured N_0 value was 0.241, which is close to the producer's value of 0.25.

Membrane electrode for H_2-O_2 fuel cell was prepared by sandwiching the Nafion 211 membrane with the cathode and anode. The catalyst "ink" was prepared by dispersing the catalysts (Fe/N/C for cathode and 40 wt% Pt/C from Johnson-Matthey for anode) in alcohol with 5 wt% Nafion solution (DuPont). The Nafion content in the catalyst layer was about 40 wt %. The loading of the catalyst was 2 mg/cm² for the cathode (Fe/N/C) and and 0.3 mg/cm² for the anode (40 wt% Pt/C), respectively. The flow rate of H_2 and O_2 was 150 mL/min.

Results and Discussion

The preparation of the PVP-NaCl-Fe/N/C is illustrated in Fig. 1a. Firstly, a supersaturated NaCl solution with PVP and $FeCl_3$ dissolved was heated at 80℃ for a while to evaporate off the water. Then the NaCl confined precursor was pyrolyzed under Ar. It needs to mention that the fast and simple confining process can be attributed to the highly hydrosoluble property of PVP, which can guarantee the homogeneous dispersion of PVP in the supersaturated NaCl solution and avoid precipitation and agglomeration as the water evaporates off rapidly. The transmission electron microscope (TEM, Fig. 1b and 1c) and scanning electron microscope (SEM, Fig. S1) images of PVP-NaCl-Fe/N/C show that carbon plates with multi-layers of carbon sheets were obtained through pyrolysis with NaCl confinement. Many pore channels and wrinkles can be seen in the thin carbon sheet (Fig. 1d), which can make the catalytic sites fully exposed and enhance the mass transfer in the catalyzing process. The materials obtained in the absence of NaCl confinement show morphology of much larger and thicker plates than PVP-NaCl-Fe/N/C (Fig. S1).

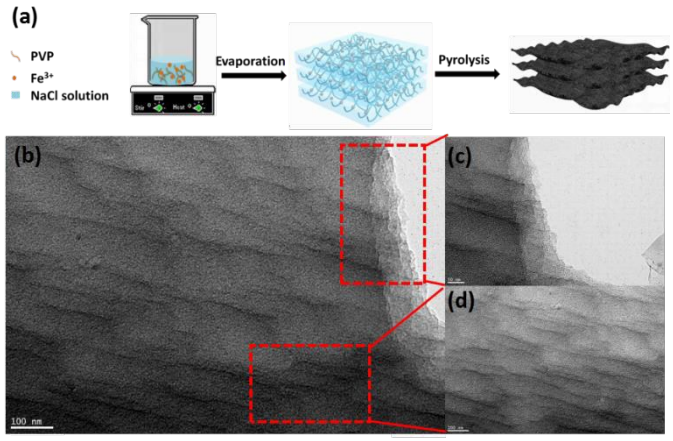

Fig.1 (a) Schematic illustration of the synthesis of the PVP-NaCl-Fe/N/C catalyst; (b) Representative TEM image of PVP-NaCl-Fe/N/C; (c) and (d) enlarge images of the corresponding square region marked in (b).

Thermogravimetric analysis (TGA) measurements were carried out to monitor the pyrolyzing process of PVP-Fe-NaCl (mixture of PVP and $FeCl_3$ sealed by NaCl) and PVP-Fe (direct mixture of PVP and $FeCl_3$ without NaCl). As depicted in Fig. 2a, PVP-Fe-NaCl shows excellent thermal stability, starting to lose weight at 400℃ which is much higher than that of PVP-Fe (about 290℃). Moreover, only 8.8% of the original weight of PVP-Fe-NaCl was lost when the temperature increased to 800 ℃ before the melting of NaCl,[40] while PVP-Fe lost 85.2% of its weight, demonstrating the effective confining of PVP inside the NaCl crystal.

The nitrogen adsorption-desorption isotherm and pore size distribution analysis results of the prepared catalysts are displayed in Fig. 2b to examine the specific surface area and the porous texture. A typical type-IV isotherm, which is characteristic of mesoporous structure,[6] was observed for both of PVP-NaCl-Fe/N/C and PVP-Fe/N/C. The pore size distribution (inset) suggested that the pore diameters for both of PVP-NaCl-Fe/N/C and PVP-Fe/N/C are centered narrowly to about 5 nm, indicating the formation of uniform pore structure by pyrolyzing PVP. A large Brunauer-Emmett-Teller (BET) surface area of 414.5 $m^2\ g^{-1}$ was obtained for PVP-NaCl-Fe/N/C , which is much larger than that of PVP-Fe/N/C (72.9 $m^2\ g^{-1}$) and the reported value for the Fe/N/C through pyrolysis of PANI and $FeCl_3$ sealed in NaCl (265.7 $m^2\ g^{-1}$),[40] proving again the effective confining of the appropriately selected PVP precursor. Raman spectroscopy was employed to characterize the carbon structure and graphitic qualities of the as-synthesized samples. The D band is usually associated with defects and disorder, and the G band corresponds to graphitic structure.[43] As shown in Fig. 2c, the D band (1340 cm^{-1}) to G band (1590 cm^{-1}) ratio (I_D/I_G) of PVP-NaCl-Fe/N/C is much lower than that of PVP-Fe/N/C, indicating a higher degree of graphitization due to the NaCl confining effect.

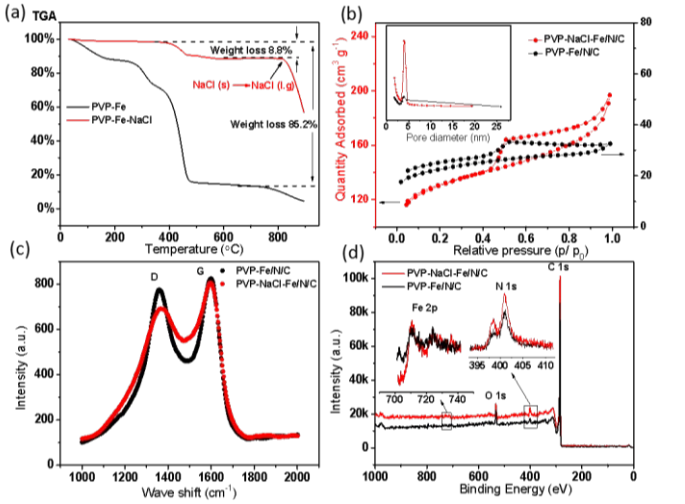

Fig. 2 Physical characterization results of PVP-NaCl-Fe/N/C and PVP-Fe/N/C: (a) TGA curves, (b) N_2 adsorption/ desorption isotherm and pore size distribution, (c) Raman spectra and (d) XPS survey and high-resolution spectra of Fe 2p and N 1s.

X-ray photoelectron spectroscopy (XPS) was carried out to investigate the composition of the catalysts. As plotted in Fig. 2d, the survey spectra demonstrate the presence of C, Fe, N, O in both PVP-NaCl-Fe/N/C and PVP-Fe/N/C. The Fe and N contents were determined to be 0.34 at.% and 4.03 at.% for PVP-NaCl-Fe/N/C, as well as 0.31 at.% and 3.23 at.% for PVP-Fe/N/C (Table 1). In other words, PVP-NaCl-Fe/N/C contains similar amounts of Fe but higher amounts of N. This fact can correspond to the TGA analysis that a much smaller weight loss occurred for PVP-NaCl-Fe than PVP-Fe, suggesting that confining PVP in NaCl can prevent the N loss during the pyrolysis.

Table 1 XPS element contents of the catalysts (at %)

	C	O	Fe	Total N	Pyridinic N	Graphitic N	Oxidized N
PVP-Fe/N/C	91.6	4.86	0.31	3.23	32.7	54.5	12.8
PVP-NaCl-Fe/N/C	91.8	3.82	0.34	4.03	33.1	59.5	7.4

High resolution spectra of Fe 2p and N 1s show similar chemical states of Fe and N for the two catalysts (inset of Fig. 2d). As depicted in Fig. S2, the N1s XPS spectra for PVP-NaCl-Fe/N/C and PVP-Fe/N/C both can be deconvolved into pyridinic (498.3 eV), graphitic (400.9 eV) and oxidized nitrogen (403 eV).[27, 38] As for the contents of different N species, PVP-NaCl-Fe/N/C possesses higher contents of pyridinic and graphitic N and much lower content of N oxide (Table 1). This agrees with the Raman results.

As expected from the high surface area, the high graphitizatio, and the high pyridinic and graphitic N contents, the prepared PVP-NaCl-Fe/N/C catalyst exhibited remarkable electrocatalytic activity for the ORR in both acidic and alkaline electrolytes. The ORR performance was first evaluated through cyclic voltammogram (CV) measurements in 0.1 M $HClO_4$ at a scan rate of 100 mV s^{-1}. As depicted in Fig. S3, an apparent oxygen reduction peak at 0.7 V (vs. RHE) was observed for PVP-NaCl-Fe/N/C in O_2-saturated $HClO_4$, as well as 0.62 V for PVP-Fe/N/C, suggesting superior ORR activity for PVP-NaCl-Fe/N/C. In addition, the PVP-NaCl-Fe/N/C exhibited several times larger of current density than that of the PVP-Fe/N/C, which should be attributed to the larger specific surface area of PVP-NaCl-Fe/N/C, in accordance with the results of BET analysis.

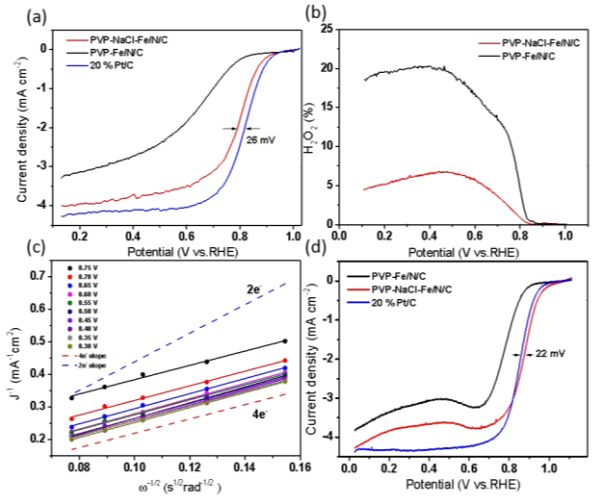

Fig. 3 (a) ORR polarization curves of PVP-Fe/N/C, PVP-NaCl-Fe/N/C and 20 wt% Pt/C (Johnson-Matthey) in O_2-saturated 0.1 M $HClO_4$. Scan rate: 5 mV s^{-1}; rotation speed: 900 rpm. (b) H_2O_2 yields of PVP-Fe/N/C and PVP-NaCl-Fe/N/C. (c) Koutecky-Levich plots for the PVP-NaCl-Fe/N/C at various potentials. (d) ORR polarization curves of PVP-Fe/N/C, PVP-NaCl-Fe/N/C and 20 wt% Pt/ C in O_2-saturated 0.1 M KOH. Scan rate: 5 mV s^{-1}; rotation speed: 900 rpm.

RDE measurements were conducted to further characterize the ORR activity of the as-prepared catalysts. The polarization curves and the corresponding Tafel plots for the catalysts are illustrated in Fig. 3a and Fig. S4, respectively. A background correction has been implemented on the polarization curves by subtracting the corresponding voltammetric responses of the same catalyst in Ar-saturated solution at the same potential scanning rate. The PVP-NaCl-Fe/N/C showed much enhanced ORR activity than PVP-Fe/N/C in respect to the onset and half-wave potential. Also, the Tafel slope (derived from the polarization curve) of PVP-NaCl-Fe/N/C was calculated to be 91 mV/ dec, much lower than that of PVP-Fe/N/C (193 mV/ dec). The lower Tafel slope given by PVP-NaCl-Fe/N/C should be due to the higher degree of graphitization as suggested by the Raman spectra, which would lead to enhanced electric conductivity. For electrocatalytic process taking place in a thin film of catalysts, the electron transport (conduction) and electron transfer (reaction) are closely coupled together, which contribute simultaneously to the apparent reaction kinetics. The ORR half-wave potential ($E_{1/2}$) of PVP-NaCl-Fe/N/C was only 26 mV negative than that of a commercial Pt/ C catalyst (20 wt% Pt, Johnson Matthey). In addition, a low H_2O_2 yield of ~ 6.7 % on PVP-NaCl-Fe/N/C electrode was detected (Fig. 3b). On the contrary, the H_2O_2 yield on PVP-Fe/N/C electrode could reach up to ~ 21 %. In a word, the confining of PVP in NaCl crystal functions effectively.

To gain more insight into the kinetics of ORR, RDE measurements at different electrode rotating speeds were carried out (Fig. S5a and Fig. S5c), based on which the Koutecky-Levich (K-L) plots at various potentials were derived. As shown in Fig. 3c, the slopes calculated from 0.3 V to 0.75 V are nearly parallel to the theoretical slope expected for a 4e- catalyzing process (dotted red line in Fig. 3c) and quite different from that of a 2e- process, inferring an approximate 4e- catalyzing process. The electron transfer number of PVP-NaCl-Fe/N/C electrode calculated from the K-L plots was determined to be 3.6 to 4.0 in the potential range of 0.3-0.75 V (Fig. S5b and Fig. S5d), further suggesting a nearly four-electron pathway for the catalysis of ORR and coinciding with the low H_2O_2 yield on PVP-NaCl-Fe/N/C catalyst. Moreover, the ORR catalytic activity in alkaline electrolyte (0.1 M KOH) was evaluated through cyclic voltammogram at a scan rate of 5 mV s^{-1}. As illustrated in Fig. 3d, the half-wave potential of PVP-NaCl-Fe/N/C (0.878 V) was ca. 22 mV more positive than that of commercial Pt/C catalysts (catalyst loading: 150 μg Pt/C cm^{-2}). These results are even better or comparable to those of the best non-precious metal catalysts reported so far (table S1, see supporting information), suggesting that the as-prepared PVP-NaCl-Fe/N/C can function as an efficient ORR catalyst.

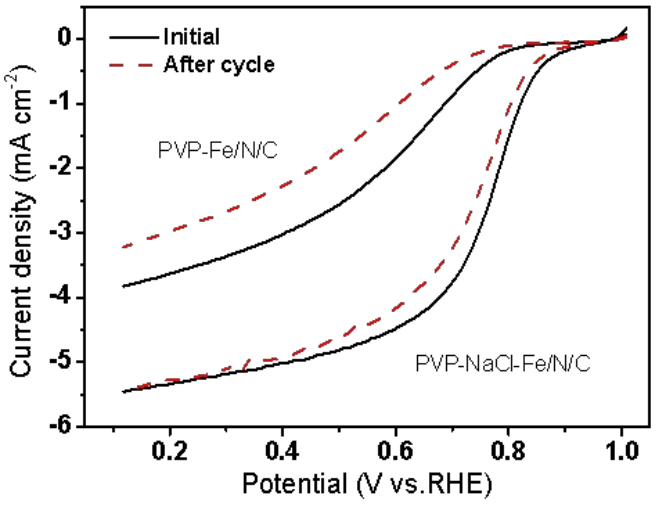

Fig. 4 ORR polarization curves for PVP-Fe/N/C and PVP-NaCl-Fe/N/C before and after cycling in O2-saturated 0.1 M HClO4 at a scan rate of 50 mV s-1.

The stability of the as-prepared catalysts was tested by cycling the electrode in the potential range of 0.1-0.9 V in O_2-saturated 0.1 M $HClO_4$ at 50 mV s^{-1}. This potential range (0.1-0.9 V) was a valid working section for the Fe/N/C catalysts when applied to the fuel cells as cathodes. In addition, O_2 other than N_2 atmosphere was employed during the stability test, since O_2 atmosphere should be the real condition for ORR electrocatalysis. As observed in Fig. 4, PVP-NaCl-Fe/N/C exhibited much enhanced cycling stability than PVP-Fe/N/C. After cycling for 1500 cycles, the half-wave potential had negatively shifted 29 mV for PVP-NaCl-Fe/N/C, much less than 100 mV observed in PVP-Fe/N/C. And the enhanced stability may benefit from the relatively high degree of graphitization, larger surface area and the homogeneous dispersion of the active sites.

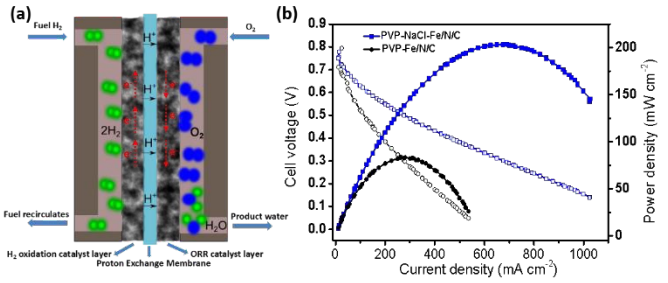

Fig. 5 (a) Schematic depiction of H_2-O_2 PEMFC. (b) Polarization (open symbols) and power density curves (filled symbols) for H_2-O_2 PEMFC with PVP-NaCl-Fe/N/C and PVP-Fe/N/C as cathode at 80 ^{o}C under a back pressure of 1 bar.

We also compared the performance of the PVP-NaCl-Fe/N/C and PVP-Fe/N/C in a H_2-O_2 PEMFCs (Fig. 5a), with the cathode made of PVP-NaCl-Fe/N/C or PVP-Fe/N/C (2 mg cm^{-2}) and anode made of 40 wt% Pt/C (0.3 mg Pt per cm^2). For the PVP-NaCl-Fe/N/C, a maximum power density of 202 mW cm^{-2} was achieved at a current density of 625 mA cm^{-2} (Fig. 5b), which were more than twice lager than that exhibited by the PVP-Fe/N/C (82 mW cm^{-2} power density at a current density of 290 mA cm^{-2}). It needs to mention that the fuel cell performances shown in Fig. 6b are just the preliminary results and subject to optimization of the MEA fabrication technique and operation conditions. These results were presented here just to further demonstrate the effectiveness of the NaCl-crystallite confinement in promoting the electrocatalytic properties of the pyrolysis-derived Fe/N/C materials.

Conclusions

By selecting a highly hydrosoluble polymer as the N-containing precursor, the pyrolysis preparation of Fe/N/C catalysts can be greatly facilitated and improved with the NaCl-crystallite confining method. The compatibility between the PVP and NaCl enables facile and uniform dispersion of precursor in NaCl crystallites, which results in much reduced nitrogen loss during the pyrolysis and high graphitization of the obtained catalyst, therefore much enhanced catalytic activity towards the ORR as compared with the materials obtained through ordinary pyrolysis.

Acknowledgements

This work was supported by the Ministry of Science and Technology of China under the National Basic Research Program (Grant nos. 2012CB215500 and 2012CB932800).

Notes and references

1. M. Lefèvre, E. Proietti, F. Jaouen and J.-P. Dodelet, Science, 2009, 324, 71-74.
2. M. Zhou, H.-L. Wang and S. Guo, Chem. Soc. Rev, 2016, 45, 1273-1307.
3. Q. Wang, Z.-Y. Zhou, Y.-J. Lai, Y. You, J.-G. Liu, X.-L. Wu, E. Terefe, C. Chen, L. Song, M. Rauf, N. Tian and S.-G. Sun, J. Am. Chem. Soc, 2014, 136, 10882-10885.
4. X. Yuan, L. Li, Z. Ma, X. Yu, X. Wen, Z.-F. Ma, L. Zhang, D. P. Wilkinson and J. Zhang, Sci. Rep, 2016, 6, 20005.
5. H. Zhu, S. Zhang, D. Su, G. Jiang and S. Sun, Small, 2015, 11, 3545-3549.
6. J.-C. Li, S.-Y. Zhao, P.-X. Hou, R.-P. Fang, C. Liu, J. Liang, J. Luan, X.-Y. Shan and H.-M. Cheng, Nanoscale, 2015, 7, 19201-19206.
7. U. I. Kramm, I. Herrmann-Geppert, J. Behrends, K. Lips, S. Fiechter and P. Bogdanoff, J. Am. Chem. Soc, 2016, 138, 635-640.
8. G. Zhang, B. Y. Xia, X. Wang and X. W. Lou, Adv. Mater, 2014, 26, 2408-2412.
9. W. Wang, Y. Zhao and Y. Ding, Nanoscale, 2015, 7, 11934-11939.
10. L. Zhao, X.-L. Sui, J.-L. Li, J.-J. Zhang, L.-M. Zhang and Z.-B. Wang, ACS Appl. Mater. Interfaces, 2016.
11. Y. Nie, L. Li and Z. Wei, Chem. Soc. Rev, 2015, 44, 2168-2201.
12. S. Zhang, B. Liu and S. Chen, Phys.Chem. Chem. Phys, 2013, 15, 18482-18490.
13. W.-J. Jiang, L. Gu, L. Li, Y. Zhang, X. Zhang, L.-J. Zhang, J.-Q. Wang, J.-S. Hu, Z. Wei and L.-J. Wan, J. Am. Chem. Soc, 2016, 138, 3570-3578.
14. Y. Chen, R. Ma, Z. Zhou, G. Liu, Y. Zhou, Q. Liu, S. Kaskel and J. Wang, Adv. Mater. Interfaces, 2015, 2, 1500199.
15. R. Zhou and S. Z. Qiao, Chem. Commun, 2015, 51, 7516-7519.
16. H. Jin, H. Huang, Y. He, X. Feng, S. Wang, L. Dai and J. Wang, J. Am. Chem. Soc, 2015, 137, 7588-7591.
17. C. Li, X. Han, F. Cheng, Y. Hu, C. Chen and J. Chen, Nat Commun, 2015, 6.
18. Y.-C. Wang, Y.-J. Lai, L. Song, Z.-Y. Zhou, J.-G. Liu, Q. Wang, X.-D. Yang, C. Chen, W. Shi, Y.-P. Zheng, M. Rauf and S.-G. Sun, Angew. Chem. Int. Ed, 2015, 54, 9907-9910.
19. H. B. Yang, J. Miao, S.-F. Hung, J. Chen, H. B. Tao, X. Wang, L. Zhang, R. Chen, J. Gao, H. M. Chen, L. Dai and B. Liu, Sci Adv, 2016, 2, e1501122.
20. G. Wu, J. Wang, W. Ding, Y. Nie, L. Li, X. Qi, S. Chen and Z. Wei, Angew. Chem. Int. Ed, 2016, 55, 1340-1344.
21. W. T. Hong, M. Risch, K. A. Stoerzinger, A. Grimaud, J. Suntivich and Y. Shao-Horn, Energy. Environ. Sci, 2015, 8, 1404-1427.
22. J.-I. Jung, M. Risch, S. Park, M. G. Kim, G. Nam, H.-Y. Jeong, Y. Shao-Horn and J. Cho, Energy. Environ. Sci, 2016, 9, 176-183.
23. X. Su, J. Liu, Y. Yao, Y. You, X. Zhang, C. Zhao, H. Wan, Y. Zhou and Z. Zou, Chem. Commun, 2015, 51, 16707-16709.

24. J. Xiao, C. Chen, J. Xi, Y. Xu, F. Xiao, S. Wang and S. Yang, Nanoscale, 2015, 7, 7056-7064.
25. L. Ding, X. Dai, R. Lin, H. Wang and J. Qiao, J Electrochem Soc, 2012, 159, F577-F584.
26. Q. Liu, H. Zhang, H. Zhong, S. Zhang and S. Chen, Electrochim. Acta, 2012, 81, 313-320.
27. W. Niu, L. Li, X. Liu, N. Wang, J. Liu, W. Zhou, Z. Tang and S. Chen, J. Am. Chem. Soc, 2015, 137, 5555-5562.
28. A. Zitolo, V. Goellner, V. Armel, M.-T. Sougrati, T. Mineva, L. Stievano, E. Fonda and F. Jaouen, Nat. Mater, 2015, 14, 937-942.
29. Y. Wang, Y. Nie, W. Ding, S. G. Chen, K. Xiong, X. Q. Qi, Y. Zhang, J. Wang and Z. D. Wei, Chem. Commun, 2015, 51, 8942-8945.
30. W. Yang, X. Yue, X. Liu, L. Chen, J. Jia and S. Guo, Nanoscale, 2016, 8, 959-964.
31. S. Zhang, H. Zhang, Q. Liu and S. Chen, J. Mater. Chem. A, 2013, 1, 3302-3308.
32. R. Jasinski, Nature, 1964, 201, 1212-1213.
33. Q. Jia, N. Ramaswamy, H. Hafiz, U. Tylus, K. Strickland, G. Wu, B. Barbiellini, A. Bansil, E. F. Holby, P. Zelenay and S. Mukerjee, ACS Nano, 2015, 9, 12496-12505.
34. S. Gupta, D. Tryk, I. Bae, W. Aldred and E. Yeager, J. Appl. Electrochem, 1989, 19, 19-27.
35. C. H. Choi, H.-K. Lim, M. W. Chung, J. C. Park, H. Shin, H. Kim and S. I. Woo, J. Am. Chem. Soc, 2014, 136, 9070-9077.
36. R. Wu, S. Chen, Y. Zhang, Y. Wang, Y. Nie, W. Ding, X. Qi and Z. Wei, J. Mater. Chem. A, 2016, 4, 2433-2437.
37. J. K. Dombrovskis and A. E. C. Palmqvist, Fuel Cells, 2016, 16, 4-22.
38. M. Xiao, J. Zhu, L. Feng, C. Liu and W. Xing, Adv. Mater, 2015, 27, 2521-2527.
39. R. Ning, C. Ge, Q. Liu, J. Tian, A. M. Asiri, K. A. Alamry, C. M. Li and X. Sun, Carbon, 2014, 78, 60-69.
40. W. Ding, L. Li, K. Xiong, Y. Wang, W. Li, Y. Nie, S. Chen, X. Qi and Z. Wei, J. Am. Chem. Soc, 2015, 137, 5414-5420.
41. J. Pampel and T.-P. Fellinger, Adv. Energy Mater, 2016, 6, n/a-n/a.
42. G. Wu, K. L. More, C. M. Johnston and P. Zelenay, Science, 2011, 332, 443-447.
43. M. Liu, Y. Song, S. He, W. W. Tjiu, J. Pan, Y.-Y. Xia and T. Liu, ACS Appl. Mater. Interfaces, 2014, 6, 4214-4222.

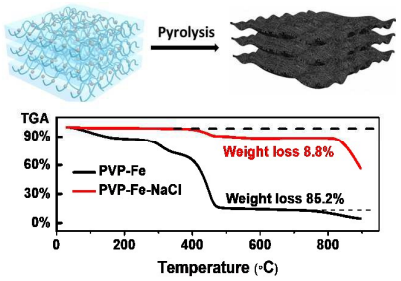

NaCl crystallites confinement can efficiently avoid the weight loss of precursor in the pyrolysis synthesis of Fe/N/C ORR catalyst.